Horn-Schunck and a Polynomial Model for Satellite Attitude Estimation

Riffi Mohammed Amine¹*   **Chouraqui Samira¹**

¹Computer Science Department, University of Sciences and Technologies of Oran, Oran, Algeria
* Corresponding author's Email: riffi.amine@ univ-usto.dz

Abstract: Estimating the Remote Sensing Satellite's Attitude variation is crucial during the acquisition in order to avoid distortions in images. This paper focuses more specifically on a method based on the Horn-Schunck (HS) multi-image recording technique associated with a piecewise polynomial model (HS-P) to estimate any variation in the attitude of satellite, and thus correct the images having undergone geometric distortion caused by slight variations in satellite attitude during acquisition taken by push-broom cameras. This linear sensor is a charge coupled device (CCD) that captures a 1-D image at a time. It is generally integrated on a platform, which moves perpendicular to its axis in time, and all the 1-D images combined form a 2-D image. The proposed method was tested on a sequence of dimensional images (400 × 800) pixels captured by the LANDSAT-ETM7 satellite. Obtained result show that the proposed approach gave satisfactory results with attitude error estimation rate of 95% and a correction of distorted images at 98%. To show the potential of our formulation considering the efficiency and the precision, the studied attitude estimation method presented was validated and compared with the LK-P differential method and other methods based on filtering techniques such as HSO-SVSPF and HORCKF.

Keywords: Remote sensing, Push-broom cameras, Linear sensor, Satellite attitude, Horn and Schunck, Polynomial model by pieces.

Nomenclature

HS	Horn-Schunck
HS-P	Horn-Shunck and a piecewise Polynomial model
CCD	Charge Coupled Device
D	Dimension
LK-P	Lucas-Kanade and a piecewise
TM	Polynomial model Thematic Maper
MD	Differential Methods
MC	Correlation Methods
HSO-SVSPF	Huber Second-order Variable Structure Predictive Filter for Satellites
HORCKF	Higher-Order Robust Correlation Kalman Filter

1. Introduction

The rise of satellite imagery technologies is manifested by a marked growth in the production of satellite images. To maintain the accurate pointing of the sensors of satellite earth observation cameras to the specified target location, an exact attitude estimate and a control system are essential.

The attitude of a satellite is defined by its three axes and their intersection form the Euler Angles [1] (Fig. 1).

- The x-axis, called the roll axis, a unit of orbital speed, tangent to the orbit.
- The axis y of the pitch, unit of the angular moment, normal to the trajectory
- The z axis called the yaw axis, along the geocentric

Today, Earth observation satellites mainly carry push broom cameras [2,3], this linear sensor can record more than 25,000 pixels on a single line of 1-D images and uses the scrolling of the satellite around the earth to create bands of images [4].

Satellites have so far been considered stable due to their inertia. Indeed a satellite is subjected to a multitude of forces and disturbing phenomena [5],
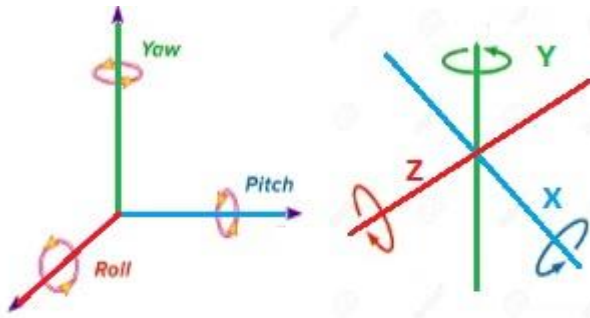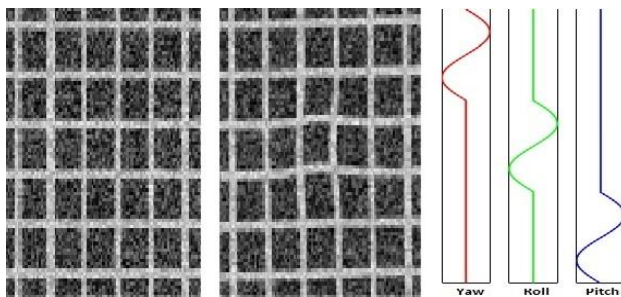
Figure. 1 The Euler angles

Figure. 2 The Example of deformations observed on a regular checkerboard when the attitude of the push-broom camera varies during the acquisition

such us the brake by the atmosphere, the irregularity of the terrestrial magnetic field, the vibrations linked to the motors and the improvement of the resolution of the sensors, which makes the imager's oscillation much more critical [6, 7]. These elements exert torques and make any solid body rotate, which causes the angles of Euler to tilt: the yaw varies the inclination of the horizontal lines; the roll oscillates the vertical lines and the pitch increases or decreases the height of the pixels (Fig. 2).

These cumulative factors mean that a change in attitude of certain micro-radians can cause significant geometric deformations in the acquired images. Therefore, the need for a good estimation of the attitude of the satellite and a better correction of the distorted image are crucial [8], which is the main contribution of this document.

In this paper, we opted for a HS method [9, 10], in order to estimate the variations in attitude of the satellite using a multi-image registration [11]. These attitude variations will be modeled by a piecewise polynomial model [12], in order to have a corrected image similar to the real image of the ground.

HS-P method is characterized by the following parameters: the number of iterations and the smoothing parameters for the HS methods, the size of the window and the number of polynomials for the polynomial model. The results are optimized by

varying the values of these parameters. The advantage of this method is to provide a dense flux (a result for each pixel) and to minimize the weighted sum of the error in the optical flux and the variation of the speed from one pixel to another by using a smoothing constraint to have a more fluid set of solutions. Polynomial offers a good estimate of low frequencies with an acceptable improvement in verisimilitude performance in terms of precision and calculation time.

This approach is more applicable for the estimation of the satellite attitude error and gives better results for the correction of distorted images compared to other methods such as differential methods (LK-P) or methods which use filtering techniques (HSO-SVSPF) and (HORCKF), the proposed approach does not involve a costly calculation and gives a very low error rate without the need for regularization parameters, which the determination is often difficult. This article is organized as follows: Section 2 presents the work related to our research theme. Section 3 describes the proposed approach. Section 4 presents and reproduces the experimental results of this work; in section 5, the results obtained are compared with the LK-P, HSO-SVSPF and HORCKF methods. Finally, Section 6 draws conclusions.

2. Related works

The field of attitude control is one of the most studied in the field of space vehicle design and which has been increasingly developed in recent work:

In 2019, Lu Cao et al. [13], authors have presented a new approach to estimate the high precision attitude of satellites using the Huber technique. This technique develops a new predictive filter with a second order variable structure. The filter can ensure a perfect estimation precision for the attitude of the satellite and stabilizes the measurement error and its difference.

Xiaoqian Chen et al [14]. Have proposed an approach to reach the estimation attitude of satellites by preliminary deriving a Kalman filter with robust correlation of higher order with unknown modelling errors using the principle of orthogonal sequence. It has been proved that the proposed filter gives better results accuracy and robustness of the estimate. This modified filter can capture the information of the probability density function of the posterior system.

In order to improve the accuracy of the attitude control system for observation satellites and to estimate its variations, Zhao-Xiang Zhang et al. [15], have proposed a new framework which merges gyroscope and tracking measurements stars with a

79

registration of the images. The calibration, gyroscopic polarization drift and star tracking error are defined by the derivative of the Kalman filter. The new frame is tested with realistically simulated data and satellite remote sensing images.

Jiang Yong-hua et al. [16], have proposed a method based on parallel observations with high-resolution push-broom cameras in order to examine the feasibility of an attitude error correction of the Chinese satellite ZY1- 02C. It contains an attitude measurement system very limited in precision, which caused complex distortions in the images, obtained and many errors in the attitude transfer.

Alexandru-RazvanLuzi et al. [17], have used jet wheels as a satellite attitude control technique. They have put in place control laws that vary according to the operating conditions. In particular, it looks for correctors ensuring a fast response when the attitude error is weak, while limiting the control effort when the satellite is far from its set position.

Perrier et al. [18], have proposed a Lucas Kanade multi-image registration method associated with a piecewise polynomial model of attitude variations. Allowing to estimate any variation of attitude of the satellite in order to rectify the acquired images.

However, the calculation of the optical flow (OF) is an essential step to estimate any satellite attitude variation. The OF estimation method proposed by Horn and Schunck has been used in the problem of movement estimation.

Enric Meinhardt-Lopis et al. [19], have described an implementation of the original HS method and have introduced a multi-scale strategy in the form of a pyramidal structure of subsampled images to manage larger displacements and create an equation optical flux constraint by a nonlinear formulation.

A.Rafael et al. [20], have developed a numerical scheme based on the technique of HS, they have proposed a new regularization algorithm based on the symmetric gradient of the flow and which is discussed in terms of invariance. To show the efficiency and accuracy of this algorithm, he compared this method with the traditional HS algorithm.

A.Matías. Molina et al. [21], have proposed a new method, which combines the differential method of HS, and the exhaustive "variational" method of Steinbücke. With the use of the full image and a volume of costs, they have managed to obtain a reduction in the processing time of exhaustive methods close to 98% compared to a similar implementation in Matlab.

unfortunatly, the abovementioned methods are sensitive to initialisation and they are also unable to analyse images with intensity inhomogeneity. Hence, these limitations abviously limit their practical applications. Here we focus in overcoming these drawbacks in this paper.

3. Proposed approach

In this paper, the implemented simulations use a sequence of images taken by the different push-broom sensors. The first TM1 image has been taken as the ground truth reference whose values angles (Roll, Yaw and Pitch) are considered exact values of the satellite. We will first illustrate our proposed approach, by following the different steps (Fig. 3).

4. Modeling

Let C the set of images taken by push-broom Channels, θ the set of radiometric values of each channel. Each pixel of each image is referenced by its coordinates $[x, y]$, and belong to the set E.

T_{ij} is the time that interspace the capture of the same scene by push-broom channels i and j. Assuming that the speed of constant satellite, in the ideal case of the attitude of a satellite is given by:

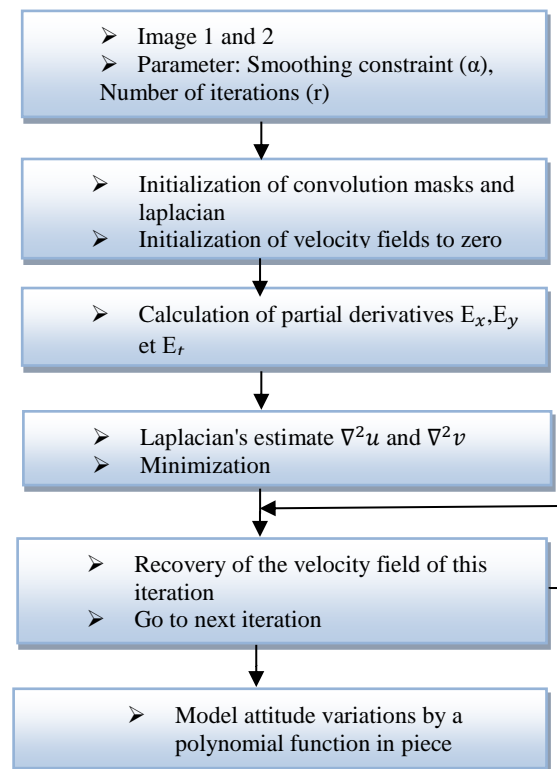$$C_i(x,y) - \mathrm{F}_{ij}\left(C_j(x + T_{ij}, y)\right) \sim \mathbb{N}(0, \sigma^2) \qquad (1)$$

Figure. 3 Different steps of the global HS method associated with the piecewise polynomial model

Where, $F_{ij} : \theta \to \theta$ is a linear function whose role is to compensate for radiometric differences between images i and j, $\mathbb{N}(0, \sigma^2)$ denotes a Gaussian function of zero (0) mean and noise variance σ^2. $C_j^{T_{ij}}$ designates the image C_j shifted in time. Eq. (1) can be written in another way as following:

$$C_i(Y) - F_{ij}\left(C_j^{T_{ij}}(Y)\right) \sim \mathbb{N}(0, \sigma^2) \qquad (2)$$

We call K the vector $(3D \times 1)$ that gathers the attitude for every moment of time and $K(x) \in \Theta$ the unknown attitude of the satellite for the moment of time which x is a vector (3×1) whose respective components are $K_\alpha(x)$ or α corresponds respectively to Yaw: $K_l(x)$, Roll: $K_r(x)$ and Pitch: $K_t(x)$.

$$K = [K_l(1)..K_l(D), K_r(1)..K_r(D), K_t(1)..K_t(D)]^T \qquad (3)$$

Let $\beta : H \times \Theta \to H$ be the deformation function containing the variations of attitude that have parasitized the images and that moves the pixel to a new position according to the attitude of the satellite from Eq. (2):

$$C_i\left(\beta(Y; K(x))\right)$$
$$-F_{ij}\left(C_j^{T_{ij}}\left(\beta\left(Y; \beta(x + T_{ij})\right)\right)\right) \sim \mathbb{N}(0, \sigma^2) \qquad (4)$$

It is important to note here that the two images are distorted by K, but for different time instants.

4.1 Retiming of multi-temporal images by the method of Horn and Schunck

A common technique for solving Eq. (4) is the Horn and Schunck method, in order to evaluate the displacement of each pixel, HS used the Lagrange multiplier method to minimize a weighted sum of the error in the optical flow and the variation of the speed from one pixel to another [20, 21]:

$$u(x, y, t), v(x, y, t)$$
$$= arg \min_{u,v} \int \left(e_b^2(u, v) + \alpha e_c^2(u, v)\right) dxdy \qquad (5)$$

Where α : is a parameter that controls the smoothing constraint, it is low for a fluid movement and high for a less smooth movement. It acts as a lubricant, where on each iteration it smooths out to produce the best movement of the optical flow

e_b: Error in the equation of the optical flow.
e_c: Pixel-to-pixel variation of speed.

$$E(x, y, t) = E(x + \delta x, y + \delta y, t + \delta t) \qquad (6)$$

Eq. (6) is the luminosity distribution of a point (x, y) in the plane of the image at time t. The luminosity of a particular point taken in the plane of the image such as: $\frac{dE}{dt} = 0$

Using the rule of the chain of differentiation Eq. (6) will become:

$$\frac{\partial E}{\partial x}\frac{dx}{dt} + \frac{\partial E}{\partial y}\frac{dy}{dt} + \frac{\partial E}{\partial t} = 0 \qquad (7)$$

By posing $u = \frac{dx}{dt}$ and $v = \frac{dy}{dt}$ we then notice that we have a linear equation two strangers u and v

$$E_x u + E_y v + E_t = 0 \qquad (8)$$

E_x and E_y are additional abbreviations for partial derivatives of brightness of the image compared to x, y and t respectively. Eq. (8) can be written in another way:

$$(E_x, E_y).(u, v) = -E_t \qquad (9)$$

The component of the movement in the direction of the gradient (E_x, E_y) is equal to: $-\frac{E_t}{\sqrt{E_x^2 + E_y^2}}$

However, it is impossible to define the component of movement that forms a right angle with the component in the direction of the gradient. The flow velocity (u, v) cannot be calculated without the integration of new constraints: smoothing constraint.

4.1.1. Smoothing constraint

The optical flow must be smooth or continuous; it is therefore assumed that neighboring points on a rigid surface have locally displacement vectors approximately identical. This amount to minimize the following error functional:

$$\left(\frac{\partial u}{\partial x}\right)^2 + \left(\frac{\partial u}{\partial y}\right)^2 \text{ and } \left(\frac{\partial v}{\partial x}\right)^2 + \left(\frac{\partial v}{\partial y}\right)^2 \qquad (10)$$

Another measure of the smoothing of the optical flow is the sum of the squares of the Laplacian components x and y of the flow. The Laplacian of u and v are defined as follows:

$$\nabla^2 u = \frac{\partial^2 u}{\partial x^2} + \frac{\partial^2 u}{\partial y^2} \quad and \quad \nabla^2 v = \frac{\partial^2 v}{\partial x^2} + \frac{\partial^2 v}{\partial y^2} \quad (11)$$

In simple situations, the two Laplacians are void. If the observer is positioned parallel to a flat object, turns around a line perpendicular to the surface or travel orthogonally with respect to the surface, then the partial second derivatives of u and v will disappear. We will use here the square of the amplitudes of the gradient as a measure of smoothing.

4.1.2. Estimation of partial derivatives

We must estimate the drifts of the brightness of the series of discrete measurements available from the image. It is important that the estimates of E_x, E_y and E_t are compatible. That means they should all refer to the same point of the image at the same time.

$$E_x \approx \frac{1}{4}\{E_{i,j+1,k} - E_{i,j,k} + E_{i+1,j+1,k} - E_{i+1,j,k} +$$
$$E_{i,j+1,k+1} - E_{i,j;k+1} + E_{i+1,j+1,k+1} - E_{i+1,j,k+1}\}$$

$$E_y \approx \frac{1}{4}\{E_{i+1,j,k} - E_{i,j,k} + E_{i+1,j+1,k} - E_{i,j+1,k} +$$
$$E_{i+1,j,k+1} - E_{i,j;k+1} + E_{i+1,j+1,k+1} - E_{i,j+1,k+1}\}$$

$$E_x \approx \frac{1}{4}\{E_{i,j,k+1} - E_{i,j,k} + E_{i+1,j,k+1} - E_{i+1,j,k} +$$
$$E_{i,j+1,k+1} - E_{i,j+1,k} + E_{i+1,j+1,k+1} - E_{i+1,j+1,k}\}$$
$$(12)$$

4.1.3. Laplacian's estimate

In order to estimate the Laplacians of u and v. A method of approaching these values takes the following form:

$$\nabla^2 u \approx K(\bar{u}_{i,j,k} - u_{i,j,k})$$
$$and \quad \nabla^2 v \approx K(\bar{v}_{i,j,k} - v_{i,j,k}) \quad (13)$$

Or the local averages $\bar{u}$ and $\bar{v}$ are defined as follows:

$$\bar{u}_{i,j,k} = \frac{1}{6}\{u_{i-1,j,k} + u_{i,j+1,k} + u_{i+1,j,k} + u_{i,j-1,k}\}$$
$$+ \frac{1}{12}\{u_{i-1,j-1,k} + u_{i-1,j+1,k}$$
$$+ u_{i+1,j+1,k} + u_{i+1,j-1,k}\}$$
$$\bar{v}_{i,j,k} = \frac{1}{6}\{v_{i-1,j,k} + v_{i,j+1,k} + v_{i+1,j,k} + v_{i,j-1,k}\}$$
$$+ \frac{1}{12}\{v_{i-1,j-1,k} + v_{i-1,j+1,k}$$
$$+ v_{i+1,j+1,k} + v_{i+1,j-1,k}\}$$
$$(14)$$

4.1.4. Minimization

The problem then, is to minimize the sum of the errors in the equation of the rate of change of the brightness of the image.

$$e_b = E_x u + E_y v + E_t \qquad (15)$$

The measurement of the error in the flow velocity pixel-to-pixel.

$$e_c^2 = \left(\frac{\partial u}{\partial x}\right)^2 + \left(\frac{\partial u}{\delta y}\right)^2 + \left(\frac{\partial v}{\partial x}\right)^2 + \left(\frac{\partial v}{\partial x}\right)^2 \qquad (16)$$

We will choose an appropriate weighting factor, noted α^2, let be the total error to be minimized:

$$e^2 = \iint (\alpha^2 e_c^2 + e_b^2)\, dxdy \qquad (17)$$

The minimization consists of finding suitable values for the optical flow rate (u, v). By using the calculation of the variations, we obtain:

$$E_x^2 u + E_x E_y v = \alpha^2 \nabla^2 u - E_x E_t$$
$$E_x E_y u + E_y^2 v = \alpha^2 \nabla^2 v - E_y E_t \qquad (18)$$

Using the Laplacian approximation introduced in the previous section:

$$(\alpha^2 + E_x^2)u + E_x E_y v = (\alpha^2 \bar{u} - E_x E_t)$$
$$(\alpha^2 + E_y^2)v + E_x E_y u = (\alpha^2 \bar{v} - E_y E_t) \qquad (19)$$

The determinant of the coefficient of the matrix is equal to: $\alpha^2(\alpha^2 + E_x^2 + E_y^2)$

The resolution for u and v gives us (diagonalization on the left):

$$(\alpha^2 + E_x^2 + E_y^2)u = (\alpha^2 + E_y^2)\bar{u} - E_x E_y \bar{v} - E_x E_t$$
$$(\alpha^2 + E_x^2 + E_y^2)v = (\alpha^2 + E_x^2)\bar{v} - E_x E_y \bar{u} - E_y E_t$$
$$(20)$$

This equation can be written in the following form:

$$(\alpha^2 + E_x^2 + E_y^2)(u - u) = -E_x[E_x \bar{u} + E_y \bar{v} + E_t]$$

$$(\alpha^2 + E_x^2 + E_y^2)(v - \bar{v}) = -E_y[E_x \bar{u} + E_y \bar{v} + E_t]$$
$$(21)$$

This shows that the value of the flow velocity (u, v), which minimizes the error e^2 lies

along a line in the direction of the stress line intersecting it at right angles.

4.1.5. Iterative solution

We use the iterative Gauss-Seidel methods; we can calculate a new set of velocity fields (u^{n+1}, v^{n+1}) from the derivatives and the average of the estimates of the previous fields (u^n, v^n) as follows:

$$\begin{aligned} u^{n+1} &= u^n - E_x \left[E_x \bar{u}^n + E_y \bar{v}^n + E_t \right] \\ &\quad / \left(\alpha^2 + E_x^2 + E_y^2 \right) \\ v^{n+1} &= \bar{v}^n - E_y \left[E_x \bar{u}^n + E_y \bar{v}^n + E_t \right] \\ &\quad / \left(\alpha^2 + E_x^2 + E_y^2 \right) \end{aligned} \qquad (22)$$

It is important to note that the estimated flow values at a specific point do not immediately depend on previous estimates of the same point.

4.2 Piecewise polynomial model

To model the variations of the attitude, it is appropriate to do polynomial interpolation in pieces where each polynomial is linked to its neighbors by constraints [12, 23].

Call $T_{T_{i,j}}$ the operator who shifts the samples of K by a factor $T_{i,j}$, this operator is a hollow matrix $(3D, 3D)$, which for each line $x \in [1, 3D]$ and column $y \in [1, 3D]$ is:

$$\begin{aligned} &T_{T_{i,j}}(x, y) = \\ &\begin{cases} 1 \; pour \, x = y - T_{i,j}, etx \notin \,]D - T_{i,j}, D] \; \cup \\ \quad]2D - T_{i,j}, 2D] \cup \,]3D - T_{i,j}, 3D] \\ 0 \quad Others \end{cases} \end{aligned} \qquad (23)$$

The general equation to be minimized is this:

$$\begin{aligned} \hat{K} = \underset{K}{argmin} \sum_{i,j; i \neq j} \sum_{Y \in E} \Bigg(C_i \big(\beta(Y; K) \big) - \\ F_{ij} \left(C_i^{T_{i,j}} \left(\beta \left(Y; T_{T_{i,j}} K \right) \right) \right) \Bigg)^2 \end{aligned} \qquad (24)$$

$P_{b,\alpha} b \in [1, S]$, S is the number of polynomials necessary to restore the attitude variations.

n_b for $b \in [1, S-1]$ the moment of time or constraints between two polynomials are defined.

The variations of attitude:

$$K_\alpha(n) = \sum_{b=1}^{S} w_b(n) P_{b,\alpha}(n) \qquad (25)$$

Where $w_b(n)$ corresponds to the weighting functions such as:

$$w_b(n) = \begin{cases} 1 \; for \, n \in [n_{b-1}, n_b] \\ 0 \; others \end{cases} \qquad (26)$$

Directly estimating K from Eq. (24) is a bad problem if no constraint is defined to direct minimization. It would be possible to add a priori on K in the equation to be minimized

The polynomials of orders M are defined such that:

$$P_{b,\alpha}(n) = \sum_{m=0}^{M} a_{m,b,\alpha} \, n^m \qquad (27)$$

The coefficients $a_{m,b,\alpha}$ characterize the variations of the attitude.

$a :$ is the vector $(3SM \times 1)$ that contains the set of polynomial coefficients.

The constraints between each polynomial at the point n_b, $b \in [1, S-1]$ are:

$$P_{b,\alpha}^{(m)}(n_b) = P_{b+1,\alpha}^{(m)}(n_b), \text{ for } m \in [0, M-1] \qquad (28)$$

Eq. (14) imposes continuity at points n_b for the derivatives until the order $M - 1$. This equation defines the constraints of linear equality in a, so we have the following matrix equation:

$$Ga = 0 \qquad (29)$$

Or G is a hollow matrix of size $(3(S-1)M \times 3SM)$ and 0 is the zero vector of dimension $(3(S-1)M \times 1)$. The combination of linear Eq. (25), Eq. (26) and Eq. (27) gives us the following matrix equation:

$$K = Ha \qquad (30)$$

Where H is a hollow matrix of size $(3D \times 3SM)$.

We can reformulate Eq. (24) by minimizing a nonlinear equation under constraint of linear equalities:

$$\begin{aligned} \hat{a} = \underset{a}{argmin} \sum_{i,j; i \neq j} \sum_{Y \in E} \Bigg(C_i \big(\beta(Y, Ha) \big) - \\ F_{ij} \left(C_i^{T_{i,j}} \left(\beta \left(Y; T_{T_{i,j}} Ha \right) \right) \right) \Bigg)^2 \end{aligned} \qquad (31)$$

Such that $C_a = 0$.

Table 1. Details about LANDSAT ETM-7 satellite

	Bands	Spatial resolution (meter)	Wavelength (micrometer)
Landsat 7 EnhancedThematic Mapper Plus (ETM+)	TM1-Blue	30	0.45-0.52
	TM2Green	30	0.52-0.60
	TM3-Red	30	0.63-0.69
	TM4- NIR	30	0.77-0.90
	TM5-SWIR 1	30	1.55-1.75
	TM6-Thermal	60	10.40-12.50
	TM7-SWIR 2	30	2.09-2.35
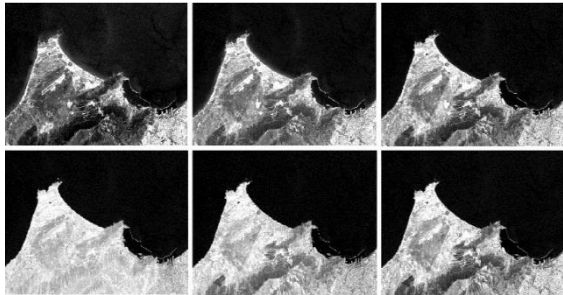
Figure. 4 the Landsat ETM-7 dataset

5. Experiment

To test the studied approach, a sequence of dimensional multispectral images (400×800) pixels of the Oran region are used. This region is located in the west of Algeria, captured by the LANDSAT ETM-7 satellite (Fig. 4). The details about these datasets are shown in (Table 1). The images TM1 represent the real terrain and is considered as the reference image in our tests. The images TM2, TM3, TM4, TM5 and TM7 are the distorted images captured by push-broom cameras. The resolution of the TM6 image is higher than the reference image resolution, so this image is not considered in tests.

The implemented algorithm depends on four parameters: The value of the degree "M", the size of the polynomial windows, value of the parameter "α" and the number of iterations. The parameter "α" controls the smoothing constraint, its value is between 0 and 1. In the data set, the velocity vector field (u_0, v_0) is initialized to zero and the cameras 1-2 are respectively spaced 10 time samples ($T_{12} = 10$).

The piecewise polynomial model applies well in our estimation context. The residual error always exists in the form of high frequency components. This is mainly due to the choice of window size when estimating. More than the size of the window is small more than the components at high frequencies are well restored. On the contrary, more than this window is large more than the components at low frequencies are restored (Table 2).

It can be seen experimentally that the choice of a high degree polynomial penalizes the method, the computing time increases, the numerical system therefore becomes unstable, as well as the difference in value between the first to the last window is important, which destabilizes solving numerically of the problem . Polynomials of degrees 2 or 3 with window sizes between 10 and 15 is often enough to eliminate this difficulty. After several tests, we set the degree M to 3 and the size of the polynomial windows to 15 time samples since they have generally produced better results in most cases and the recording has good sub-pixel accuracy and most of the low frequencies are restored.

We make soft alpha "α" towards 0 and the number of iterations tends towards infinity to obtain a suitable result. It is noted that, it is necessary to make more iteration to detect all the moving pixels and more than the value of the smoothing constraint "α" is high and close to 1 more than we get a bad estimate and we lose precision on pixel movements. Conversely, the smaller the alpha is, the more precision you gain. After several tests, we set the value of "α" to 0.001 and the number of iterations to 40 , these values give best results of the flow velocity (u,v) in an acceptable execution time (Table 3).

The verisimilitude denotes the estimation error between the real attitude of the Euler angles Eq. (2) and its estimation provided by Eq. (5), [22].

Table 2. Results of the piecewise polynomial model on the Landsat ETM-7 dataset

canal	window size	Processing time (s)	the standard error		
			roll	yaw	pitch
TM2	5	10.09	0.56	0.45	0.27
	10	10.06	0.38	0.44	0.25
	15	10.04	0.25	0.39	0.23
TM3	5	10.09	0.58	0.83	1.23
	10	10.06	0.39	0.81	0.94
	15	10.04	0.29	0.79	0.89
TM4	5	10.09	0.53	0.97	1.25
	10	10.06	0.37	0.95	1.19
	15	10.04	0.19	0.70	0.90
TM5	5	10.09	0.45	0.91	1.15
	10	10.06	0.32	0.88	0.90
	15	10.04	0.27	0.81	0.85
TM7	5	10.09	0.55	0.90	1.25
	10	10.06	0.32	0.87	0.92
	15	10.04	0.22	0.70	0.88

Table 3. Results of the HS method on the Landsat ETM7 dataset ($\alpha = 0.001$, iter = 40)

Canal	Verisimilitude			u	v
	roll	yaw	pitch		
TM2	0.1154	0.1191	0.1189	9.6837	7.1435
TM3	0.1232	0.1275	0.1123	9.6231	7.1126
TM4	0.1226	0.1173	0.1144	9.6451	6.9952
TM5	0.1178	0.1289	0.1265	9.1475	7.1235
TM7	0.1286	0.1257	0.1167	9.5478	7.1478
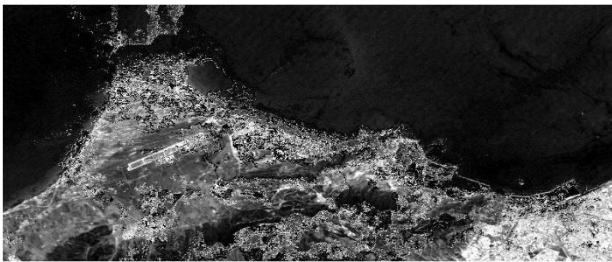
Figure. 5 TM2 distorted image
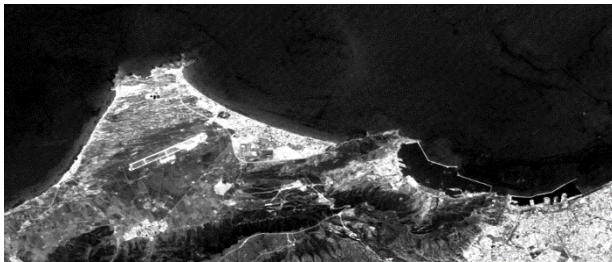
Figure. 6 TM1 reference image

After various tests carried out on all the distorted images, we have chosen as an example to show the tests, which have been carried out on TM2 (Fig.5), the image which has undergone greater deformations compared to the reference image TM1 (Fig.6).

To estimate a polynomial that models the low signal frequencies, we set the degree *M* to 3 and the size of the polynomial windows to 5, 10 and 15 time samples.

In the first test, we set the size of the polynomial windows to 5 time samples (Fig. 7). The algorithm has converged in 10.09 seconds over 40 iterations. The standard error in the estimation of the roll, yaw and pitch attitude is greater than 1/50. In the second test, we have fixed the size of the polynomial windows 15 times (Fig. 8). The algorithm converges in 10.04 seconds over 40 iterations; the standard error observed on the attitude estimation is less than 1/50 for roll, yaw and pitch. The results show the performance and the limits of our algorithm. It can be

noted that the low frequencies are fairly well estimated with an acceptable improvement in performance, likelihood of precision and of computation time with a polynomial of degree 3 and a size of the polynomial windows at 15 (Table 2 in the channel TM2).

In both cases, the residual error always contains high frequency components. This is mainly related to the choice of window size during the estimation. A small window makes it easier to restore high frequencies since the model will have more degrees of freedom. Conversely, a large window will restore well the low frequencies.
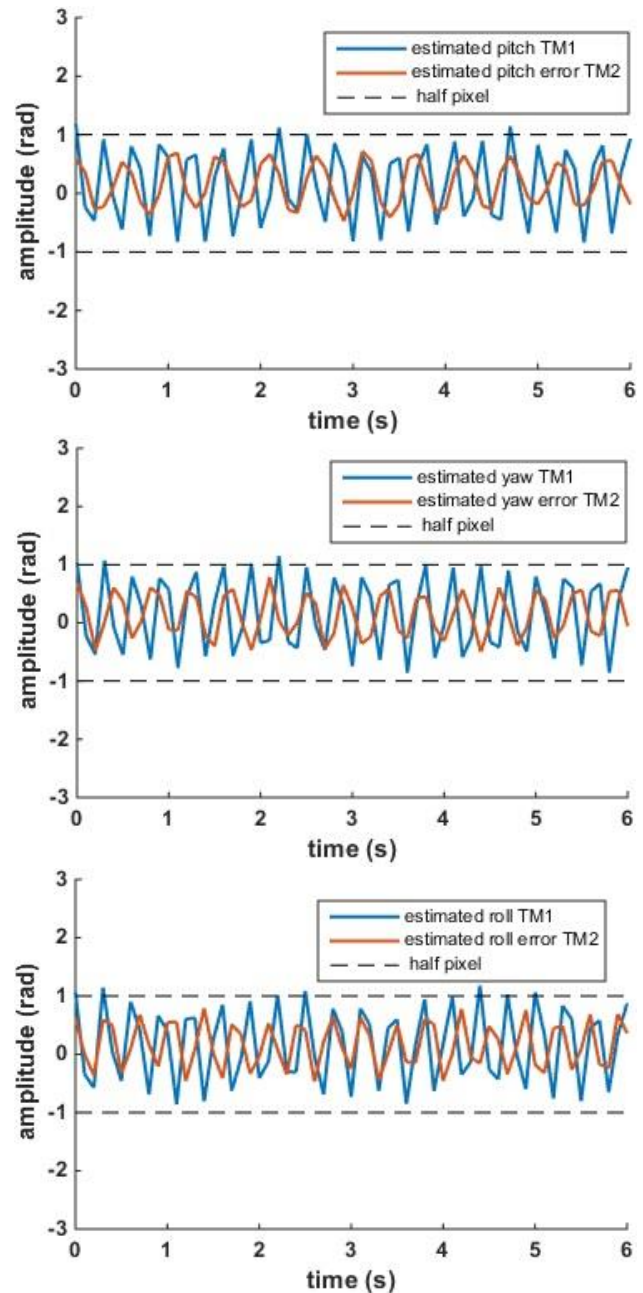

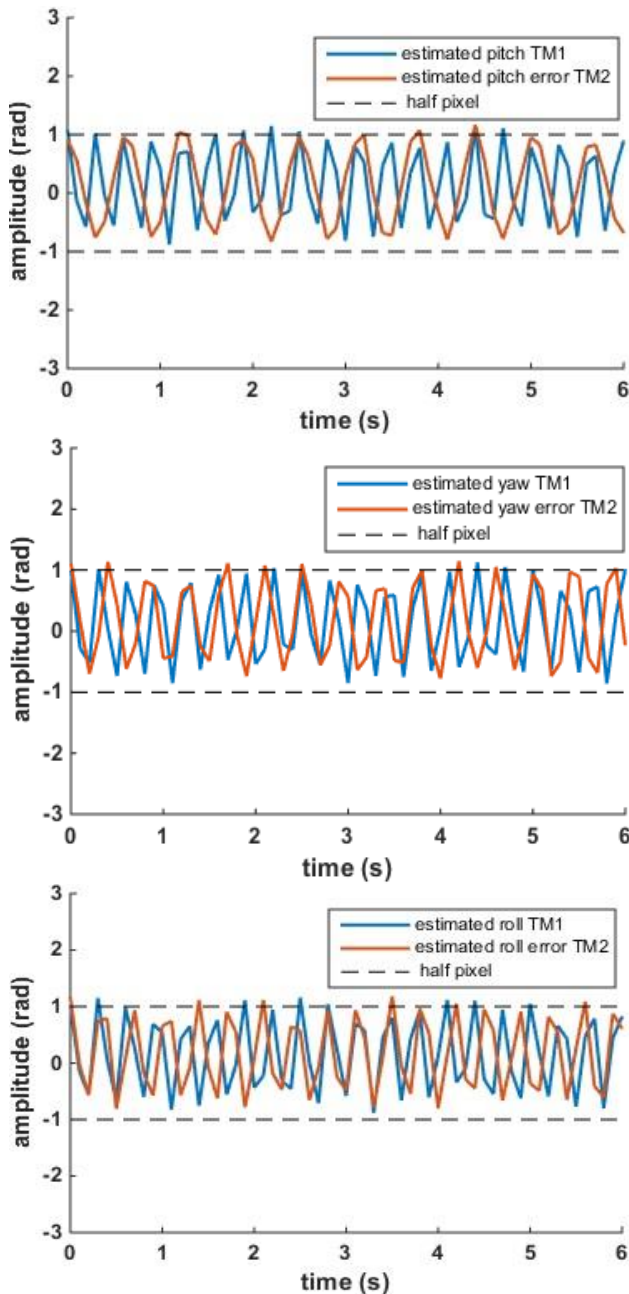Figure. 7 The pitch, yaw and roll estimation error of TM2 image (M=3, window size =5)

Figure. 8 The pitch, yaw and roll estimation error of TM2 image (M=3, window size =15)

Table 4. Results of the HS method on the TM2 image

Iteration	Verisimilitude		
	roll	yaw	pitch
20	0.2256	0.268	0.2247
30	0.1296	0.1208	0.1218
40	0.1154	0.1191	0.1189

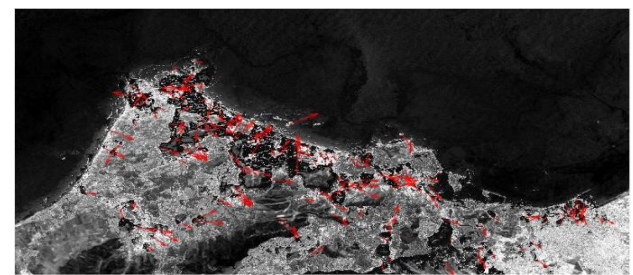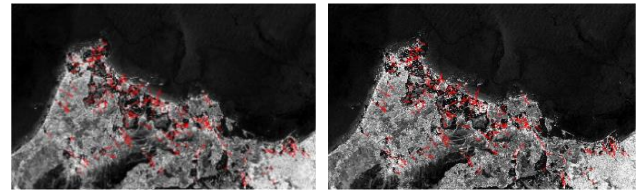(α=0.001,Iter=20)   (α=0.001, Iter=30)

(α=0.001, Iter=40): best result

Figure. 9 Tracing motion vectors using the HS method
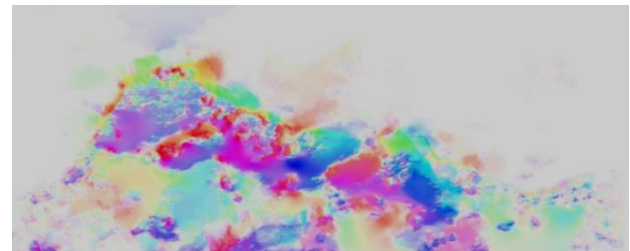
Figure. 10 representation of the speed vectors of by the color map

The resulting calculated flow is presented in the form of a needle diagram for 20, 30 and 40 iteration with *α* which equal to 0.001. The images of the(Fig. 9) show the displacement vectors estimated by the correlation method that we presented at different iteration values (Table 4).

The first test with 20 iterations. The verisimilitude of the TM2 image in roll, yaw and pitch attitude estimation error is greater than 1/20 of a pixel. The results show vectors in the direction of the brightness gradient and the speed estimates may not be very precise. Few changes occur after 30

iterations when the verisimilitude of the TM2 image in roll, yaw and pitch attitude estimation error is less than 1/20 of a pixel and the velocity vectors have errors of about 10%. The last test with 40 iterations, the vectors are very close in all parts of the image. The verisimilitude of the roll, yaw and pitch attitude estimation error is less than 12/100.

We can deduce that the more we increase the number of iterations, the verisimilitude in roll, yaw and pitch attitude estimation error is less important.

The most interesting solution is the use of the colour map, which make better representation of the way and the direction of the flow as well as its intensity in a dense (Fig. 10). We have applied this colour card on the image obtained with 40 iterations,

Table 5. Comparison of the proposed HS-P with LK-P, HSO-SVSPF and HORCKF

Author (Year)	Method	Dataset used	Verisimilitude The standard error			*u*	*v*	Processing time (s)
			roll	yaw	pitch			
/	HS-P	Landsat TM1/TM2	0.1154 **0.25**	0.1191 0.43	0.1189 **0.23**	9.6837	7.1435	38.156184
Perrier, R and al [19] (2010)	LK-P	Landsat TM1/TM2	0.1232 0.88	0.1275 0.85	0.1357 1.15	10.587	8.2547	40.254787
Chen, X and al [15] (2019)	HORCKF	Landsat TM1/TM2	0.1425 **0.90**	0.1424 **0.92**	0.1454 **1.22**	/	/	30.124763
Cao, L and al [14] (2019)	HSO-SVSPF	Landsat TM1/TM2	0.1149 0.61	0.1197 **0.39**	0.1201 0.54	/	/	39.234581

Figure. 11 Rectified image thanks to the motion vector

representing the best results. It is noticed that, they are a good estimate of the movement as a whole, with a slight blur in the discontinuity zones and a dense optical flow.

The deformation is significant before the registration of the two images where all the contours are apparent. The offset error between the two images after the attitude correction is satisfactory because the registration error is reduced overall and a few contours are apparent in the borders of the image (Fig. 11).

6. Comparison study

In order to demonstrate the efficiency and robustness of our proposed method, we have compared the performance of studied HS-P model with the LK-P differential method [18] and with methods based on filtering techniques such as HSO-SVSPF [13] and HORCKF [14]. In this comparative study, we have defined the degree M to 3, the size of the polynomial windows to 15 time samples, the value of "α" to 0.001 and the number of iterations to 40. These comparisons were tested on the Landsat TM2 distorted image.

(Table 5) shows the roll, pitch and yaw measurements, which means the standard error between the actual attitude and the attitude estimated in pixel units (the best result tends towards zero); The estimation time corresponds to the number of seconds

of execution the complete algorithm (the best is the smallest number). In each row of the table, the best score is in green and the worst in red.

In the first comparison with LK-P methods, the results obtained, have showed that the proposed algorithm HS-P gives better results of the standard error and the velocity of flow (u, v) and improves signal strength in an acceptable execution time. The polynomial model confirms its good results, but above all the scores displayed by the likelihood values are more impressive: the precision here is less than half a pixel for the HS-P, while that observed for the LK-P s close to a pixel.

In the second comparison with the HORCKF approach, we have noted that HS-P has the better ability to take into account the estimation of modeling errors than HORCKF (Fig. 12). The values obtained by the HORCKF method are not satisfactory compared to the values measured by the HS-P model. The attitude error estimates are almost equal to one, and the verisimilitude of the TM2 image in roll, yaw and pitch attitude estimation error measured are greater than 1/10. These values are not adequate for a good correction of the distorted image.

In the last comparison with the HSO-SVSPF method, we note that the two methods provide almost the same rate of estimation of the attitude error for roll and pitch; on the other hand, the best error rate attitude for the yaw is obtained with HSO-SVSPF within an acceptable execution time. The verisimilitude of the TM2 image in roll, yaw and pitch attitude estimation error measured by HS-P is better to that measure by the HSO-SVSPF ,so we can say that the precision, the estimation of attitude the computation time obtained by HS-P is better than that of HSO-SVSP (Fig. 13).

After this comparative study, we can deduce that the proposed technique is more robust and better in terms of accuracy and satellite attitude estimation
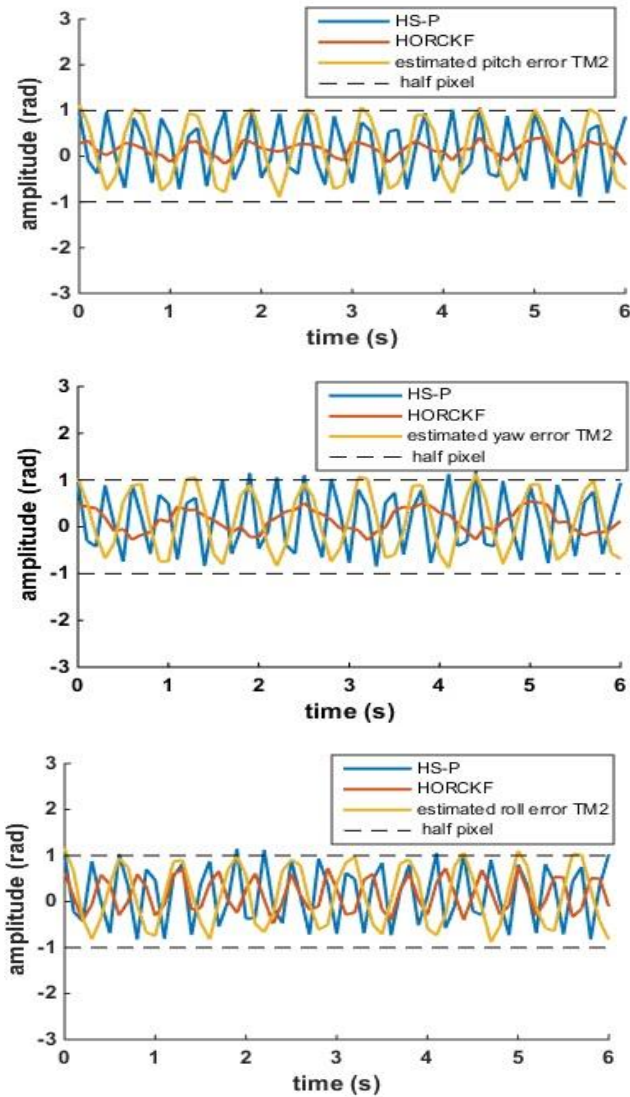
Figure. 12 The pitch, yaw and roll estimation error of TM2 image (HS-P / HORCKF)

Figure. 13 The pitch, yaw and roll estimation error of TM2 image (HS-P / HSO-SVSPF)

than existing techniques. This is due to the perfect adjustment of the smoothing parameters and the number of iterations of the HS registration method. particularly, the integration of the piecewise polynomial model with the HS registration method have allowed good modeling attitude changes with a very low error rate.

7. Conclusion

The originality of this work is based on the use of the HS-P approach, in order to estimate the attitude of a satellite from images acquired by push broom cameras. By matching the distorted images, the proposed algorithm have acquired and corrected the images.

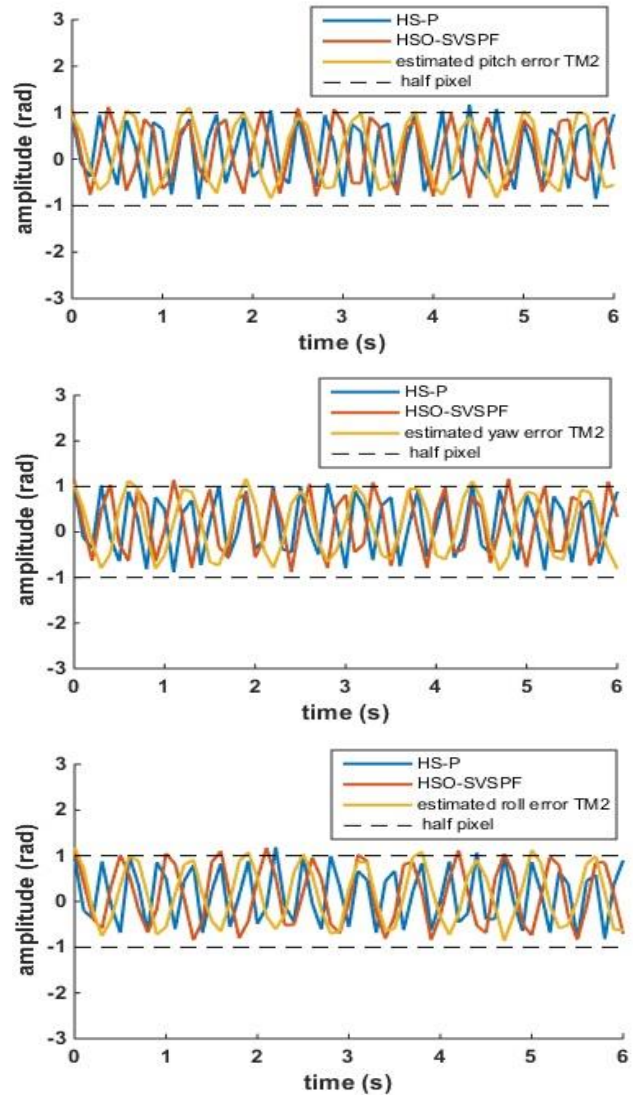The objectives have been defined since the results obtained from digital test cases confirm the feasibility and effectiveness of the technique for correctly estimating the attitude error. In addition compared to other methods of estimating attitude variation cited in section 5. The image obtained after recording is interesting especially for low frequency components, since few contours are apparent, the residues observed on the estimation of the error of the attitude are good, especially for roll, which is less than a 1/10 of a pixel. Overall, the image to be corrected is almost just relative to the reference image with a correction rate of almost 100% and an attitude error estimation rate of less than 1/2 pixel. In addition, the polynomial model used in our work has a lot of similarity with spline recording methods, so we consider it interesting and useful to extend it by applying these techniques without limiting it by introducing regularization functions. Therefore, the implementation of the proposed HS-P method can

overcome the problem of the distortion of satellite images and have them corrected after their acquisitions.

To confirm the robustness of this method and to eliminate its exact limits, we are currently looking for solutions allowing to automatically select the most suitable window size to have a good reproduction of the high frequency components.

Conflicts of Interest

The authors declare no conflict of interest.

Author Contributions

Conceptualization: Riffi Mohammed Amine and Chouraqui Samira; methodology: Riffi Mohammed Amine and Chouraqui Samira; software: Riffi Mohammed Amine; validation: Riffi Mohammed Amine and Chouraqui Samira; formal analysis: Riffi Mohammed Amine and Chouraqui Samira; Investigation: Riffi Mohammed Amine; resources: Riffi Mohammed Amine; data curation: Riffi Mohammed Amine; writing—original draft preparation: Riffi Mohammed Amine and Chouraqui Samira; writing—review and editing: Riffi Mohammed Amine and Chouraqui Samira; visualization : Riffi Mohammed Amine; supervision : Chouraqui Samira; project administration :Chouraqui Samira; no funding acquisition.

References

[1] J. Diebel, "Representing Attitude: Euler Angles, Unit Quaternions, and Rotation Vectors", *Stanford University Stanford, California*, pp. 94301-9010, 2006.

[2] J. Cazenove, "Les capteurs CCD Initiation à la théorie et à la pratique", *Bulletin de l'Union des Physiciens*, Vol. 88, No. 762, pp. 471-506, 1994.

[3] R. Gupta, Hartley, and I. Richard. "Linear pushbroom cameras", *IEEE Transactions on Pattern Analysis and Machine Intelligence*, Vol. 19, No. 9, pp. 963-975, 1997.

[4] P. Golland and A. M. Buckstein, "Motion from Color", *Computer Vision and Image Understanding*, Vol. 68, No. 3, pp. 346–362, 1997.

[5] G. Petrie, "Airborne Pushbroom Line Scanners: An Alternative to Digital Frame Cameras", *Geoinformatics*, Vol. 8, No. 1, pp. 50–57, 2005.

[6] R. Amri and D. Gibbon. "In orbit performance of butane propulsion system", *Article in Advances in Space Research*, Vol. 49, No. 4, pp. 648–654, 2012.

[7] A. M. SiMohammed, M. Benyettou, Y. Bentoutou, A. Boudjemai, Y. Hashida, and M. N. Sweeting, "Three-axis active control system for gravity gradient stabilised microsatellite", *Article in Acta Astronautica*, Vol. 64, No. 7-8, pp. 796-809, 2009.

[8] T. Iwata, "Precision attitude and position determination for the Advanced Land Observing Satellite (ALOS)", *Article in Proceedings of SPIE - The International Society for Optical Engineering*, Vol. 5659, pp. 34-50, 2005.

[9] B. K. P. Horn and B. G. Schunck, "Determining Optical Flow", *Technology, Cam- bridge, MA 02139, U.S.A. Artificial Intelligence*, Vol. 17, No. 1–3, pp. 185-203, 1981.

[10] K. Jaiganes, M. S. Siti, I. Norazlin, H. Aini, and M. M. Mohd, "Motion detection using Horn Schunck algorithm and implementation", In: *Proc. of the International Conference on Electrical Engineering and Informatics*, Selangor, Malaysia, pp. 83-87, 2009.

[11] L. Brown. "A survey of image registration techniques", *ACM Computing Surveys*, Vol. 24, No. 4, pp. 325-376, 1992.

[12] M. Unser, "Splines: A perfect fit for signal and image processing", *IEEE Signal Processing Magazine*, Vol. 16, No. 6, pp. 22-38, 1999.

[13] L. Cao, D. Ran, X. Chen, X. Li, and B. Xiao, "Huber second-order variable structure predictive filter for satellites attitude estimation", *International Journal of Control, Automation and Systems*, Vol. 17, No. 7, pp. 1781-1792, 2019.

[14] X. Chen, L. Cao, P. Guo, and B. Xiao. "A higher-order robust correlation Kalman filter for satellite attitude estimation", *ISA Transactions*, 2019.

[15] Z. Zhang, X. G. D. Xu, and J. N. Song, "Observation satellite attitude estimation using sensor measurement and image registration fusion", *Proceedings of the Institution of Mechanical Engineers, Part G: Journal of Aerospace Engineering*, Vol. 232, No. 7, pp. 1390-1402, 2018.

[16] Y. H. Jiang, G. Zhang, X. Tang, D. Li, and W. C. Huang, "Detection and correction of relative attitude errors for ZY1-02C". *IEEE Transactions on Geoscience and Remote Sensing*, Vol.52, No.12, pp.7674-7683, 2014.

[17] Alexandru Razvan Luzi. " Commande Variante dans le Temps pour le Contrôle d'Attitude de Satellites", *Automatique / Robotique. Institut Supérieur de l'Aéronautique et de l'Espace - ISAE,* 2014.

[18] R. Perrier, E. Arnaud, P. Sturm, and M. Ortner, "Satellite image registration for attitude estimation with a constrained polynomial model", In: *Proc. of International Conference on Image Processing*, Hong Kong, pp. 925-928, 2010.

[19] E. M. Llopis, J. S. Pérez, and D. Kondermann, "Horn-schunck optical flow with a multi-scale strategy", *Image Processing Online*, pp. 151-172, 2013.

[20] R. A. Bonfim, D. E. Queiroz, G. A. Giraldi, P. J. Blanco, and R. A. Feijoo, "Determining Optical Flow using a Modified Horn and Schunck's Algorithm", *System*, Vol. 3, pp. I2, 2010.

[21] A. M. Molina and G. V. Lazcano, "Matlab programmed method for the optical flow estimation based on the integral image", In: *Proc. of the 4th International Conference on Control, Automation and Robotics (ICCAR)*, Auckland, New Zealand, pp. 394-399, 2018.

[22] G. Xiaoliang and S. Bansmer, "Horn–Schunck optical flow applied to deformation measurement of a birdlike airfoil", *Chinese Journal of Aeronautics,* Vol. 28, No. 5, pp. 1305-1582, 2015.

[23] H. Pan, Z. Zou, G. Zhang, X. Zhu, and X. Tang, "High-resolution satellite imagery", *IEEE Transactions on Geoscience and Remote Sensing*, Vol. 54, No. 3, pp. 1849-1859, 2015.